Active subspaces for the optimal meanline design of unconventional turbomachinery

Bahamonde Noriega, J.S.; Pini, Matteo; Servi, Carlo De; Colonna, Piero

DOI
10.1016/j.applthermaleng.2017.08.093

Publication date
2017

Document Version
Final published version

Published in
Applied Thermal Engineering

Applied Thermal Engineering 127 (2017) 1108–1118

Contents lists available at ScienceDirect

Applied Thermal Engineering

journal homepage: www.elsevier.com/locate/apthermeng

Research Paper

Active subspaces for the optimal meanline design of unconventional turbomachinery

Sebastian Bahamonde [a], Matteo Pini [a], Carlo De Servi [a,b], Piero Colonna [a,*]

[a] Propulsion & Power, Delft University of Technology, The Netherlands
[b] Flemish Institute for Technological Research (VITO), Mol, Belgium

HIGHLIGHTS

- A reduced-order model is proposed for the design of unconventional turbomachinery.
- The surrogate combines fluid selection, cycle configuration, and turbine geometry.
- The surrogate outperforms the standard model with negligible computational cost.
- The new response surface reveals the dominant inputs for turbine performance.

ARTICLE INFO

Article history:
Received 8 March 2017
Revised 11 July 2017
Accepted 18 August 2017
Available online 19 August 2017

Keywords:
Active subspaces
Organic Rankine Cycle
Turbomachinery
Reduced-order model
Renewable energies
Turbine preliminary design

ABSTRACT

The preliminary fluid dynamic design of turbomachinery operating with non-standard working fluids and unusual operating conditions and specifications can be very challenging because of the lack of know-how and guidelines. Examples are the design of turbomachinery for small-capacity organic Rankine cycle and supercritical CO_2 cycle power plants, whereby the efficiency of turbomachinery components has also a strong influence on the net conversion efficiency of the system. These machines operate with the fluid in thermodynamic states which, for part of the process, largely deviate from those obeying to the ideal gas law. This in turn implies the presence of so-called non-ideal compressible fluid dynamics effects.

Active subspaces, a model reduction technique, is at the basis of the methodology presented here, which is aimed at the optimal meanline design of unconventional turbomachinery. The resulting surrogate model depends on a very small set of non-physical variables, called active variables. The procedure integrates into a single constrained optimization framework the selection of the working fluid, the thermodynamic cycle calculation and the preliminary sizing of the turbomachinery component.

As a demonstration of the advantages of the proposed approach, the design of a 10 kW mini organic Rankine cycle turbine with a turbine inlet temperature of 240 °C is illustrated. In this case, approximately the same maximum efficiency is estimated for three dissimilar turbines operating with different working fluids and rather different thermodynamic cycles. The use of active subspaces allows the seamless evaluation of the sensitivity of results to input parameters, both those related to the machine and the working fluid. The novel design procedure is compared in terms of computational efficiency to a conventional approach based on the coupling of a genetic algorithm directly with a meanline code. Results show that the calculation based on the use of surrogate models is more than two orders of magnitude faster. The surrogate can be used to solve any design problem within the specified boundaries of the design envelope. Results are affected by uncertainty on the estimation of losses and of non-ideal compressible fluid dynamics effects, which, in turn, do not affect the applicability of the method, which will become quantitatively accurate once this information will be available. Work to this end is underway in various laboratories.

1. Introduction

The increasing need for renewable energy conversion has boosted the development of power technologies based on thermodynamic cycles operating with unconventional fluids, e.g., the

* Corresponding author at: Propulsion & Power, Delft University of Technology, Kluyverweg 1, 2613SH, The Netherlands.
E-mail address: P.Colonna@tudelft.nl (P. Colonna).

http://dx.doi.org/10.1016/j.applthermaleng.2017.08.093
1359-4311/

Nomenclature

Symbols

$\dot{m}$	mass flow rate [kg/s]
$\dot{W}$	power [kW]
$\hat{c}_P$	non-dimensional ideal gas heat capacity at constant pressure
a	coefficients of the ideal gas heat capacity at constant pressure
a	EoS parameter
b	blade height [mm]
c_P	ideal gas heat capacity at constant pressure [kJ/kmol K]
D	diameter [mm]
h	specific enthalpy [kJ/kg]
P	pressure [bar]
R	Universal gas constant [kJ/kmol K]
r	radius [mm]
s	entropy [kJ/kg K]
T	temperature [°C]
t	time [h]
t_{cl}	tip clearance thickness [mm]
t_{te}	trailing edge thickness [mm]
U	blade peripheral speed [m/s]
w	relative flow velocity [m/s]
x_{ac}	active variables

Subscripts

0..3	turbine stage stations relative to Fig. 3
cn	condensation
cr	critical
ev	evaporation
in	inlet
m	meridional
out	outlet
r	reduced
s	isentropic
sh	superheating
sv	saturated vapor
ts	total-to-static

Greek Letter

$\alpha_{1,ge}$	stator outlet blade angle [°]
$\beta_{3,ge}$	rotor outlet blade angle [°]
χ	molecular mass [kg/kmol]
Δ	drop
ϵ	error [%]
η	efficiency [%]
γ	EoS parameter [m^3/kmol]
Ω	rotational speed [rpm]
ω	acentric factor
Ω_e	specific speed
Φ	pressure ratio
ϕ	flow coefficient
σ	molecular complexity
τ	EoS parameter
υ	molar volume [m^3/kmol]
ε	EoS parameter
φ_0	design parameter: radius ratio of the rotor outlet hub to shroud
ϑ_0	design parameter: radius ratio of rotor outlet shroud to rotor inlet

organic Rankine cycle (ORC) and the supercritical CO_2 cycle (sCO_2) [1]. In particular, R&D activities on mini ORC systems (*m*ORC, 3—50 kW) are considerably raising, because they are envisioned to play a relevant role in the decentralized energy generation scenario, and as waste heat recovery (WHR) systems for mobile engines, e.g., on board of long-haul trucks, ships, or aircraft [2–5].

The success of these technologies strongly depends on the realization of high-efficiency turbomachinery. In this respect, its preliminary design is key and particularly challenging, because the machine is bound to be unconventional, and its feasibility and manufacturability are not guaranteed. The fluid dynamic design strongly depends on the working fluid and on the cycle operating parameters, and is constrained by a considerable number of parameters related to feasibility, e.g., rotational speed, tip clearance, blade height, etc. For instance, for a turbine operating in a high-temperature *m*ORC turbogenerator, the maximum pressure ratio, and thus the cycle thermal efficiency, might be constrained by the minimum blade height at the first-stage rotor inlet; this blade height is ultimately determined by a combination of factors like the fluid volumetric flow, the turbine degree of reaction, and the inlet diameter [6]. Moreover, for WHR systems on board of transportation vehicles, additional features to be considered are the weight and volume of the heat exchangers. Although critical for *m*ORC systems, some of these challenges affect, to some extent, also the design of other more conventional ORC and $scCO_2$ systems. Here, emphasis is given to the optimal meanline design of mini-ORC turbines, but the methodology is applicable to a large variety of turbine and compressors whenever working fluids and operating conditions do not allow the use of an experience-based approach.

Generally, the preliminary fluid dynamic design stage is accomplished by following two sequential (or independent) procedures. First, the isentropic efficiency of the machine is estimated by means of similarity parameters taking into account the characteristics of the fluid process occurring in an ORC turbine: large volumetric expansion ratio, compressibility effects, and, in case of a small power output, scaling effects [7,8]. These similarity parameters are a function of the fluid thermodynamic conditions at turbine inlet and outlet. As such, they have been widely used in the design of ORC systems, see, e.g., Refs. [9–11]. Once the best working fluids are selected, the geometry of the machine is determined by means of an automated optimization process based on a meanline turbine model, which is properly initialized using the outcome of the first step. The set of equations constituting the meanline turbine model is equivalent to a highly non-linear multidimensional function, that might exhibit discontinuities. Consequently, and in order to enhance the robustness of the optimization, a gradient-free optimizer is commonly adopted, see, e.g., Refs. [12–14].

This design process is time-consuming and it can lead to suboptimal results, because it is made of subsequent procedures which have to be performed for each considered working fluid, for different turbine configurations and for a wide range of operating condition. For instance, for radial inflow turbines, the preliminary design phase requires approximately 50% of the total design time (preliminary and detailed) [15]. Furthermore, the design of mini ORC turbines is particularly challenging, given that the machine geometry and the operating conditions are mutually constrained variables, hence hampering the definition of a feasible design space. Ultimately, based on our experience, see, e.g.,Ref. [6], achieving an optimum solution of the design problem might take from weeks

to months. A further drawback follows from the use of a gradient-free optimizer: the sensitivity of expander efficiency, or of any other output of interest, to individual design inputs is lost. If available, this information can be used to gain physical understanding of loss mechanisms already at preliminary design level.

The results of a previous study demonstrated that a reduced-order model allows to overcome these disadvantages [16]. Following such development, this paper presents an innovative design methodology employing a reduced-order model which integrates fluid selection, thermodynamic cycle calculation, and preliminary fluid dynamic design of the corresponding ORC turbine.

The method is based on active subspaces, a parameter-reduction strategy that utilizes the dominant directions of the gradient of a scalar function to transform a multidimensional input space into a lower-dimensional problem [17]. The obtained surrogate is computationally efficient and robust, which makes this approach arguably preferable compared to the conventional design procedure. In addition, the resulting surface can be used to analyze the influence of the individual design inputs on the objective function. Finally, the selection of the working fluid is not limited to existing substances, because a fluid is specified by several molecular parameters, thus optimal solutions may encompass parameters that do not correspond to any available compound, but that might guide to the synthesis of a new chemical. The benefits of this approach have been demonstrated by applying it to the exemplary design of a 10 kW ORC unit for exploitation of medium-temperature thermal sources and adopting a single-stage radial inflow turbine as expander. The results and the performance of the design procedure are discussed and compared to those obtained by employing a conventional approach in order to put into evidence the main advantages.

2. Method

The design procedure integrating the thermodynamic cycle calculation, the working fluid selection, and the turbine preliminary design, consists of three steps. First, a turbine model is obtained in such a way that it includes the parameters of an equation of state model to predict the properties of the working fluid, as in

$$f = f(\mathbf{x}), \quad \mathbf{x} = [\mathbf{y}, \mathbf{z}], \quad \mathbf{x} \in [-1, 1]^m, \tag{1}$$

where $\mathbf{y}$ and $\mathbf{z}$ are vectors containing the inputs for the fluid and turbine models, respectively. Expression (1) is a scalar function to compute any quantity of interest, like, for example, the turbine total-to-static efficiency. Observe also that the inputs in $\mathbf{x}$ are centered and normalized, and that in order to construct the reduced-order model, (1) needs to be smooth [17]. The second step consists in approximating function (1) with a lower order function $\hat{f}$, i.e.,

$$f(\mathbf{x}) \approx \hat{f}(\mathbf{x}_{\mathrm{ac}}), \quad \mathbf{x}_{\mathrm{ac}} \in \mathbb{R}^n, \quad n < m, \tag{2}$$

where $\mathbf{x}_{\mathbf{ac}}$ are the so-called *active variables*. The reduced-order model is then used to obtain several response surfaces, namely one for the turbine efficiency, and one each for the main turbine operating and geometric parameters, e.g., the minimum blade height. In the third step, the surrogate model is employed to perform the optimization. Sections 2.1, 2.4 describe these steps in detail.

Eq. (1) shows that the method requires the definition of the design space $\mathbf{x}$. In order to better illustrate how $\mathbf{x}$ is defined, an exemplary application of this design method is first introduced, namely the preliminary design of a *m*ORC unit (power capacity < 20 kW) for the conversion of medium-temperature thermal sources (maximum cycle temperature $< 240\,^{\circ}$C), and adopting a single-stage radial inflow turbine. This design problem, representative of applications like waste heat recovery from long-haul truck diesel engines [2], or solar power conversion in space [18,19], is particularly challenging because the choice of system operating conditions, working fluid, and components design, are mutually constrained [16].

Fig. 1 shows the corresponding process flow diagram and an exemplary thermodynamic cycle in the temperature-entropy plane. Table 1 lists the fluids selected because they feature a critical temperature $> 240\,^{\circ}$C, and because of their high thermal stability [19].

The turbine preliminary design is performed by means of a meanline code, whose loss models are listed in Ref. [6]. These models have been developed for conventional turbomachinery operating with fluids in the ideal gas state, and featuring subsonic flows and large Reynolds numbers. The meanline code has been compared with the results of literature test cases presenting these characteristics [23]. The code has not been validated yet for the case of *m*ORC turbines because experimental data are not available yet. In this respect, work is in progress in order to be able to perform accurate measurements on mini ORC turbines [24]. Anyhow, the validity of the procedure to create a reduced-order model is not affected by the uncertainty in the loss correlations.

The preliminary design method has been implemented in a general-purpose programming environment [25], and the code can run in parallel on multiple cores. The high-order turbine model consists of a meanline program for the preliminary design of turbomachinery [26], coupled with a library for fluid property estimation, which has been extended with a fluid model especially

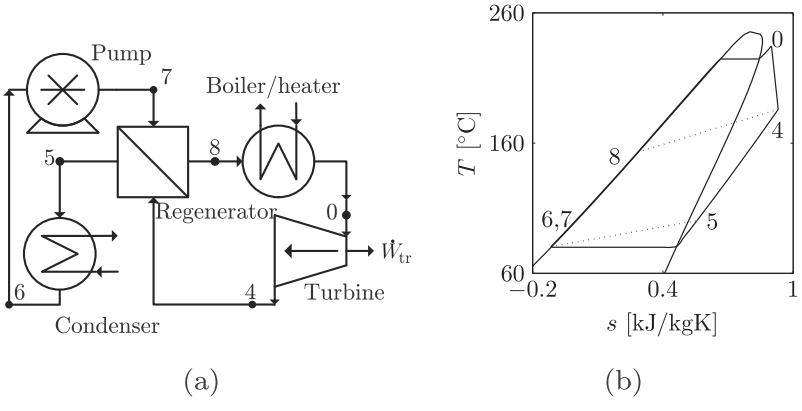

Fig. 1. (a) Process flow diagram of an ORC system with regeneration. (b) Exemplary temperature-entropy diagram of a superheated thermodynamic cycle. Working fluid: MM, condensing temperature: 80 °C, evaporating pressure: 14 bar, degree of superheating: 10 K, regenerator pinch temperature: 20 K, pressure loss: 0%, turbine isentropic efficiency: 80%.

Table 1
Molecular mass (χ), acentric factor (ω), critical pressure (P_{cr}), critical temperature (T_{cr}), and molecular complexity $\left(\sigma = \frac{T_{cr}}{R}\left(\frac{\partial s_{sv}}{\partial T}\right)_{T_r=0.7}\right)$[a] for the selected working fluids [20,21].

		χ, kg/mol	ω, –	P_{cr}, bar	T_{cr}, °C	σ, –
Toluene	C_7H_8	0.0921	0.2657	41.26	318.60	9.04
n-heptane	C_7H_{16}	0.1002	0.3490	27.36	266.98	17.56
m-xylene	C_8H_{10}	0.1062	0.3260	35.34	343.74	14.34
n-octane	C_8H_{18}	0.1142	0.3590	24.97	296.17	23.50
Hexamethyldisiloxane (MM)	$C_6H_{18}OSi_2$	0.1624	0.4180	19.39	245.55	28.14
Octamethyltrisiloxane (MDM)	$C_8H_{24}O_2Si_3$	0.2365	0.5290	14.15	290.94	48.44
Octamethylcyclotetrasiloxane (D_4)	$C_8H_{24}O_4Si_4$	0.2966	0.5920	13.32	313.34	51.89
Decamethyltetrasiloxane (MD_2M)	$C_{10}H_{30}O_3Si_4$	0.3107	0.6680	12.27	326.25	65.95
Decamethylcyclopentasiloxane (D_5)	$C_{10}H_{30}O_5Si_5$	0.3708	0.6580	11.61	346.08	73.37
Dodecamethylpentasiloxane (MD_3M)	$C_{12}H_{36}O_4Si_5$	0.3848	0.7220	9.45	355.21	92.31
Dodecamethylcyclohexasiloxane (D_6)	$C_{12}H_{36}O_6Si_6$	0.4449	0.7360	9.61	372.63	104.54
Tetradecamethylhexasiloxane (MD_4M)	$C_{14}H_{42}O_5Si_6$	0.4590	0.8250	8.77	380.05	106.39
Perfluorodecalin (PP_5)	$C_{10}F_{18}$	0.4620	0.4777	17.88	291.85	60.74
Perfluoro-2,4-dimethyl-3-ethylpentane (PP_{90})	C_9F_{20}	0.4881	0.5621	16.00	256.85	50.93

[a] For a complete discussion on the molecular complexity see Ref. [22].

developed for the application of this method [21]. The results presented here have been obtained on a Windows 64-bit computer, equipped with a 3.60 GHz processor with eight processors and 16 GB of RAM.

2.1. Working fluid model

The model must guarantee sufficiently accurate estimation of the fluid thermodynamic properties for a wide range of operating conditions and for different working fluids; yet it should feature the lowest number of parameters in order to ease the construction of the reduced-order model. Cubic equations of state (CEoS) provide a balance between these requirements [27]. Four models were initially considered: van der Waals (VDW) [28], Redlich/Kwong (RK) [29], Peng/Robinson (PR) [30], and Soave/Redlich/Kwong (SRK) [31]. All these CEoS can be written in the general form

$$P = \frac{RT}{v-\gamma} - \frac{a(T)}{(v+\varepsilon\gamma)(v+\tau\gamma)}, \tag{3}$$

where P is the pressure, T is the temperature, v is the molar volume, and R is the universal gas constant. Parameters $a(T)$, ε, γ, and τ depend on the cubic equation variant, and are a function of the temperature, acentric factor, and critical properties [27,32].

The ideal gas heat capacity at constant pressure is approximated as a function of the molecular complexity [22], defined as

$$\sigma \equiv \frac{T_{cr}}{R}\left(\frac{\partial s_{sv}}{\partial T}\right)_{T_r=0.7}, \tag{4}$$

where s_{sv} is the saturated-vapor entropy calculated at a reduced temperature of 0.7. The molecular complexity parameter is used because it is directly related to the molecular structure of the fluid, therefore to its heat capacity [22]. Starting from the definition (4), it is possible to demonstrate that σ and the corresponding heat capacity are proportional.

A fluid model can thus be expressed as a function of five parameters, i.e.,

$$\text{fluid model} = f(\chi, \omega, P_{cr}, T_{cr}, \sigma). \tag{5}$$

In order to choose the most accurate CEoS model, (3) was used to compute the saturation pressure and vapor molar volume for temperature values between 80 °C and 240 °C and for the fluids listed in Table 1. The model outputs were then compared against calculations performed with state-of-the-art fluid libraries implementing reference equation of state models [21,20]. Values calculated with the VDW and RK models were too different from those obtained with the reference models, and were thus discarded. The computation of the property values with the SRK is affected by a mean relative deviation from reference values that is lower than 4% per fluid, while those performed with the PR model yielded some deviations from reference values as high as 14%. SRK was therefore selected for implementation into the coded procedure. The addition of complex transport property models to the method is left for future developments. The viscosity employed in the estimation of stator losses [16] is taken as a constant equal to 10^{-5} Pa s.

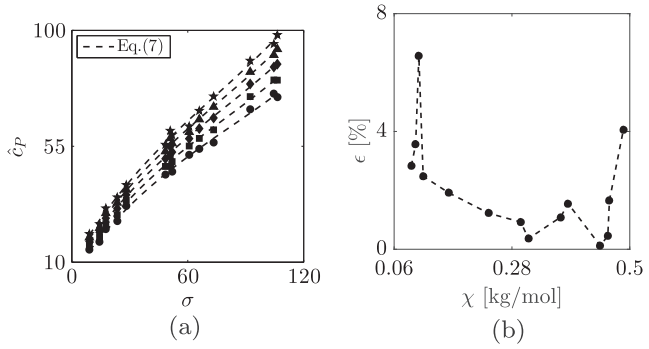

Fig. 2. (a) Non-dimensional ideal gas heat capacities for the fluids listed in Table 1 as a function of the molecular complexity and for five temperature levels: (★) $T = 240$ °C, (▲) $T = 200$ °C, (◆) $T = 180$ °C, (■) $T = 100$ °C, (•) $T = 80$ °C. (- -) Polynomial regressions for each temperature level. (b) Mean error of the approximation of the heat capacity as a function of the molar mass and for the fluids listed in Table 1.

The temperature dependence of the non-dimensional heat capacity is commonly expressed as a polynomial, i.e.,

$$\hat{c}_P = \frac{c_P}{R} = \mathbf{a}[1 \quad T \quad T^2 \quad T^3]\prime, \quad \mathbf{a} = [a_1 \quad a_2 \quad a_3 \quad a_4], \tag{6}$$

where c_P is the molar heat capacity. The coefficients in $\mathbf{a}$ are fluid dependent, and they are generally determined by experiments combined with knowledge of the fluid molecular structure [27].

In order to approximate $\mathbf{a}$ as a function of σ, five $\hat{c}_P$ samples for equidistant temperature levels between 80 °C and 240 °C are obtained for each fluid by means of reference models [20,21]; Fig. 2a shows the values obtained with the accurate models and their regression using

$$\hat{c}_P|_T \approx f(\sigma) \tag{7}$$

for each temperature. For a given σ, five $\hat{c}_P$ samples can be estimated by means of (7). These samples are then used to perform a polynomial regression and obtain $\mathbf{a}$. Fig. 2b presents the mean relative error of the estimation of the heat capacity values within

the selected temperature range, and as a function of the molecular mass of the selected fluids.

2.2. Normalized input of the turbine model for preliminary design

A meanline code for the preliminary design of turbomachinery [6,26] is coupled with the in-house computational fluid library [21] in which fluid model (5) has been implemented. Among various inputs, the design model requires the turbine rotational speed Ω, the rotor inlet diameter D_2, and the mass flow $\dot{m}$. The successful application of the active subspaces method requires that the mathematical model is continuous and differentiable, therefore Ω, D_2 and $\dot{m}$ must be normalized, such that the input parameters are fluid independent. To this purpose, the mass flow rate is computed by means of the isentropic power $\dot{W}_s$, as in

$$\dot{m} = \frac{\dot{W}_s}{\Delta h_s}, \tag{8}$$

where Δh_s is the specific isentropic expansion work. Likewise, the rotational speed is calculated with the isentropic specific speed $\Omega_{e,s}$, i.e.,

$$\Omega = \frac{\Omega_{e,s}\Delta h_s^{3/4}}{(\dot{m} v_{out,s})^{1/2}}, \tag{9}$$

where $v_{out,s}$ is the specific volume at the turbine outlet. The specific speed is therefore a design choice; results from a previous study suggest that the optimum value of $\Omega_{e,s}$ is in the range $[0.5, 0.7]$ [8].

Finally, an optimal rotor inlet diameter is estimated by means of conventional design guidelines for radial inflow turbines [33], combined with a mass balance assuming an isentropic expansion, which gives

$$D_2 = 2\left(\frac{\dot{m} v_{out,s}}{\Omega\phi\pi\vartheta_0^2(1-\varphi_0^2)}\right)^{1/3}, \tag{10}$$

where ϑ_0 is the radius ratio of the rotor outlet shroud to rotor inlet ($r_{s,3}/r_2$, see Fig. 3), and φ_0 is the radius ratio of the rotor outlet hub to shroud ($r_{h,3}/r_{s,3}$, see Fig. 3). The subscript 0 indicates that these variables are primarily inputs used to compute the rotor diameter; the turbine model ultimately provides the design values of ϑ and φ. Furthermore, (10) requires the flow coefficient

$$\phi = c_{m,3}/U_2, \tag{11}$$

which is taken equal to 0.3. In (11), $c_{m,3}$ is the meridional flow velocity at rotor outlet, and U_2 is the rotor peripheral speed.

Fig. 3 presents the meridional channel of a radial inflow turbine stage and the inputs required by the combined meanline/fluid model. Note that T_{ev}, T_{cn}, and ΔT_{sh} are used to determine the turbine inlet temperature and inlet/outlet pressure values, thus connecting the turbine model with the thermodynamic cycle calculation.

2.3. Reduced-order model with active subspaces

Ref. [17] provides a thorough review of the active subspaces method; the goal of this method is to transform the scalar function (1),

$$f = f(\mathbf{x}), \quad \mathbf{x} = [x_1, x_2, \ldots, x_m]', \quad \mathbf{x} \in [-1, 1]^m,$$

into (2), a lower-dimension approximation,

$$f(\mathbf{x}) \approx \hat{f}(\mathbf{x}_{ac}), \quad \mathbf{x}_{ac} \in \mathbb{R}^n, \quad n < m,$$

The input space of $\hat{f}$, $\mathbf{x}_{ac}$, is constituted by *active variables*, i.e., linear combinations of the input variables

$$\mathbf{x}_{ac} = \mathbf{B}\mathbf{x}, \tag{12}$$

where $\mathbf{B}$ is a $n \times m$ matrix. The active subspaces method provides a strategy to compute $\mathbf{B}$. The procedure is based on the study of matrix $\mathbf{C}$,

$$\mathbf{C} = \mathbb{E}\left[(\nabla_x f)(\nabla_x f)'\right] = \int (\nabla_x f)(\nabla_x f)\prime\rho d\mathbf{x}, \tag{13}$$

where $\mathbb{E}$ denotes the expectancy, ρ is a probability density function, and $\nabla_x f$ is the column vector of partial derivatives of f, namely,

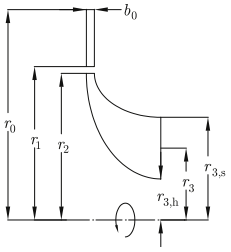

Inputs for the fluid model, $\mathbf{y}$ in (1)		Inputs for the turbine model, $\mathbf{z}$ in (1)	
Molar mass	χ	Cycle evaporating temperature	T_{ev}
acentric factor	ω	Isentropic power	$\dot{W}_{tr,s}$
Critical pressure	P_{cr}	Isentropic degree of reaction	R_s
Critical temperature	T_{cr}	Isentropic specific speed	$\Omega_{e,s}$
Molecular complexity	σ	Stator outlet blade angle	$\alpha_{1,ge}$
		Rotor outlet blade angle	$\beta_{3,ge}$
		Stator outlet/rotor inlet radius ratio	r_1/r_2
		Stator inlet/outlet radius ratio	r_0/r_1
		Rotor inlet/outlet radius ratio	r_2/r_3
		Degree of superheating	ΔT_{sh}
		Cycle condensing temperature	T_{cn}
		Tip clearance thickness	t_{cl}
		Trailing edge thickness	t_{te}
		Rotor outlet shroud to inlet radius ratio	ϑ_0
		Rotor outlet shroud to hub radius ratio	φ_0
		Flow coefficient	ϕ

Fig. 3. Inputs for the combined turbine and fluid model.

$$\nabla_x f = \left[\frac{\partial f}{\partial x_1}, \frac{\partial f}{\partial x_2}, \ldots, \frac{\partial f}{\partial x_m}\right]'. \tag{14}$$

The expectancy of a random variable x is the weighted average of all values x can take; $\mathbf{C}$ can be interpreted as the uncentered covariance of $\nabla_x f$. As such, its eigenvectors determine the directions on which f changes the most, on average [34].

If multidimensional integration is not feasible, $\mathbf{C}$ can be approximated by sampling as

$$\hat{\mathbf{C}} = \frac{1}{M}\sum_{j=1}^{M}(\nabla_x f)(\nabla_x f)', \tag{15}$$

where M is the number of samples. The sampling strategy and number of samples might affect the accuracy of this approximation; this is discussed in detail in Ref. [17]. In this case, leveraging the results of a previous study [16], the sampling was performed with a latin hypercube combined with sparse grid. The derivatives in (15) can be computed by means of finite differences. Alternatively, $\hat{\mathbf{C}}$ can be determined with local linear models [17] and these have been utilized in this work.

$\hat{\mathbf{C}}$ can be transformed by means of a real eigenvalue decomposition, because it is real and symmetric. The transformation reads

$$\hat{\mathbf{C}} = \hat{\mathbf{W}}\hat{\mathbf{\Lambda}}\hat{\mathbf{W}}', \tag{16}$$

where $\hat{\mathbf{\Lambda}}$ is a diagonal matrix containing the eigenvalues, and $\hat{\mathbf{W}}$ is a matrix containing the eigenvectors. The eigenvalues represent the magnitude of the variance of $\nabla_x f$ along their eigenvectors orientation. It follows that large gaps between eigenvalues indicate directions where f changes the most. Subsequently, these matrices can be separated in two subsets denominated active (ac) and inactive (ic), namely,

$$\hat{\mathbf{W}} = \begin{bmatrix}\hat{\mathbf{W}}_{ac} & \hat{\mathbf{W}}_{ic}\end{bmatrix}, \quad \hat{\mathbf{\Lambda}} = \begin{bmatrix}\hat{\mathbf{\Lambda}}_{ac} & \hat{\mathbf{\Lambda}}_{ic}\end{bmatrix}. \tag{17}$$

$\hat{\mathbf{\Lambda}}_{ac}$ contains the largest eigenvalues separated from $\hat{\mathbf{\Lambda}}_{ic}$ by a large gap; $\hat{\mathbf{W}}_{ac}$ contains the corresponding eigenvectors. The input space is then geometrically transformed and aligned with $\hat{\mathbf{W}}_{ac}$, in order to "hide" the directions where the function variability is small. This transformation leads to a lower-order input space formed by the active variables,

$$\mathbf{x}_{ac} = \hat{\mathbf{W}}'_{ac}\mathbf{x}. \tag{18}$$

$\mathbf{B}$ in (12) is therefore the active-eigenvector matrix $\hat{\mathbf{W}}'_{ac}$.

Because of the sampling required to approximate $\hat{\mathbf{C}}$, there are M transformations in the active subspace $\left(\hat{f} : \mathbf{x}_{ac} \rightarrow f\right)$. These samples could be used to obtain the reduced-order model by means of a regression based on any functional form. Alternatively, additional sampling might be required to cover regions with a low number of solutions.

Consider the following function as an illustrative exercise (adapted from Ref. [17]),

$$f = (0.7x_1 + 0.3x_2)^2 + 1. \tag{19}$$

Fig. 4a presents a surface plot of (19) generated with one hundred samples. Fig. 4b shows the surface top view, with the sample gradients represented by arrows, and with the corresponding active and inactive eigenvectors. The sample gradients are prominently aligned with a single orientation given by $\hat{\mathbf{W}}_{ac}$; the function variability has thus one dominant direction. Subsequently, the input space is rotated and aligned with $\hat{\mathbf{W}}_{ac}$, "hiding" the directions of low function variability, and reducing the number of model inputs to a single active variable, see Fig. 4c. Finally, by means of the available samples, a polynomial regression is realized in the active subspace, and the reduced-order model takes the functional form

$$\hat{f} = 0.6x_{ac}^2 + 1. \tag{20}$$

2.4. Optimization

Fig. 5 shows a plot of the exemplary reduced-order model (19). The minimum function value is located between $x_{ac} = -0.2$ and $x_{ac} = 0.2$. Next, the active variables in this region are transformed into inputs. This problem is undetermined because

$$x_{ac,1} = a_1x_1 + a_2x_2$$

is the only equation, but the unknowns are two, namely, x_1 and x_2. Alternatively, this system of equations can be solved by performing a random search in $\mathbf{x}$, until solutions within the region $-0.2 \leqslant x_{ac,1} \leqslant 0.2$ are found. This procedure is computationally cheap, because each transformation $\mathbf{Bx}$ takes only few milliseconds to compute.

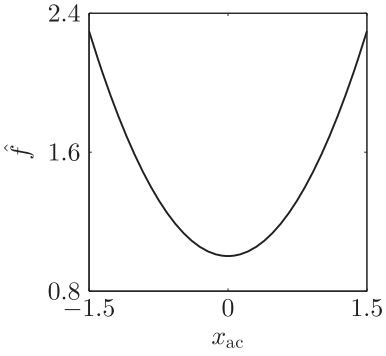

Fig. 5. Exemplary reduced-order model (20).

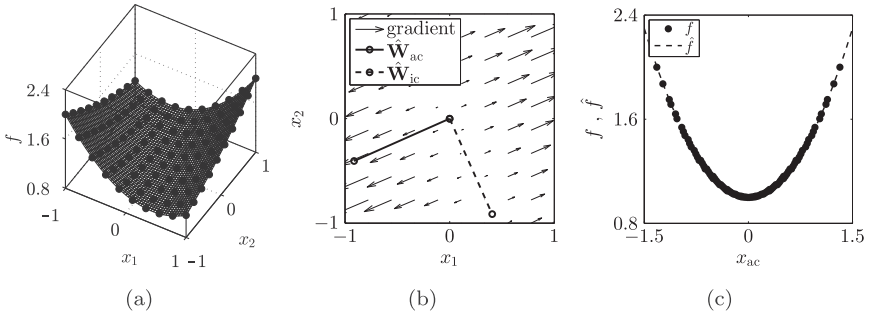

Fig. 4. Exemplary process to obtain a reduced-order model. (a) Surface plot of (19) produced with one hundred samples (•). (b) Surface top view, with the sample gradients represented by arrows, and with the corresponding active ($\hat{\mathbf{W}}_{ac}$) and inactive ($\hat{\mathbf{W}}_{ic}$) eigenvectors. (c) Reduced-order model in the active subspace, function samples (•), and functional form (20) (–). Example adapted from Ref. [17].

Table 2
Design space, constant parameters, and model outputs employed for the construction of the active subspace model.

	ω, –	χ, kg/mol	P_{cr}, bar	T_{cr}, °C	σ, –	T_{ev}, °C	R_s, –	$\alpha_{ge,1}$, °	$\beta_{ge,3}$, °	r_0/r_1, –	r_1/r_2, –	$\dot{W}_{tr,s}$, kW	$\Omega_{e,s}$, –
Minimum	0.2657	0.0921	8.77	245.55	9.04	180	0.4	65	40	1.2	1.04	10	0.5
Maximum	0.8250	0.4881	41.26	380.05	106.39	240	0.5	80	60	1.5	1.10	20	0.7
	T_{cn}, °C	ΔT_{sh}, K	t_{cl}, mm	t_{te}, mm	r_2/r_3, –	ϕ, –	ϑ_0, –	φ_0, –					
Constants	80.0	10	0.2	$0.1t_{to}$	2.0	0.3	0.7	0.4					
Outputs	$\eta_{tr,ts}$	ϑ	w_3	α_2	β_3	b_0							

2.4.1. Turbine constrained design

The meanline model is used to compute several outputs of interest, e.g., the objective of the design optimization, typically the total-to-static efficiency $\eta_{tr,ts}$, together with geometrical constraints, e.g., the radius ratio of the rotor outlet shroud to rotor inlet, $r_{s,3}/r_2$. Each output requires its own reduced-order model. The turbine meanline model can thus be transformed into a system of equations in the form

$$\text{Turbine reduced-order model} \begin{cases} \hat{\eta}_{tr,ts} & = \hat{f}(\mathbf{x}_{ac,\eta}), \\ \hat{\phi}_i & = \hat{g}_i(\mathbf{x}_{ac,\phi,i}), \quad i \in \{1,\dots,N\}, \end{cases} \tag{21}$$

where $\hat{\eta}_{tr,ts}$ is the active subspace model of the objective function, and $\hat{\phi}_i$ is the i^{th} active subspace model corresponding to a constrained output. Finally, the optimization problem reads

$$\begin{aligned} &\text{Maximize} \quad \hat{\eta}_{tr,ts}, \\ &\text{subject to} \quad \psi_{min,i} \leqslant \hat{\phi}_i \leqslant \psi_{max,i}, \quad i \in \{1,\dots,N\}, \end{aligned}$$

where $\psi_{min,i}$ and $\psi_{max,i}$ are the design constraints. The problem can be solved by exploiting the random search approach, and by taking into account that each transformation **Bx** must concurrently respect the imposed constraints; this is the method adopted in this work. Alternatively, the optimization could be performed with a genetic algorithm or a gradient-based search method, as described in Ref. [16].

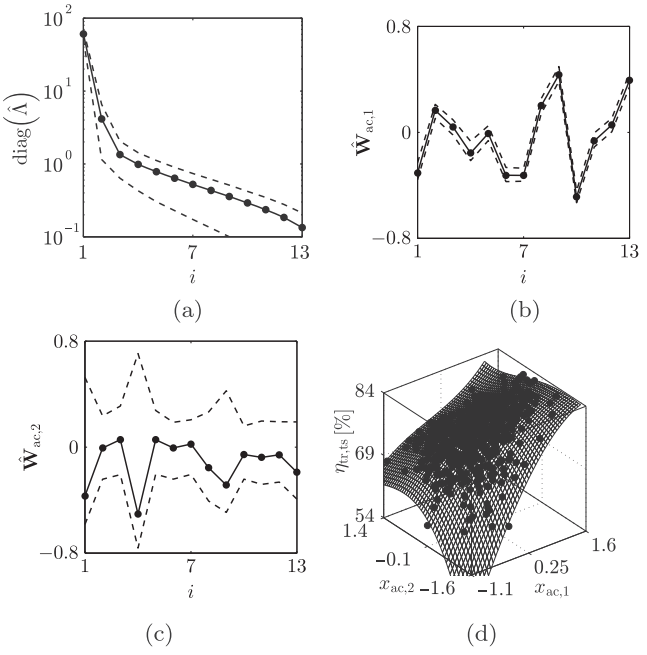

Fig. 6. (a) Eigenvalues of $\hat{\mathbf{C}}$ associated with the total-to-static efficiency function computed with the combined fluid/turbine model. The dotted lines correspond to a 95% bootstrap confidence interval computed with 10,000 samples. (b) First active eigenvector. (c) Second active eigenvector. (d) Reduced-order response surface and samples (•). See Ref. [17] for information on bootstrapping.

3. Exemplary application

Table 2 reports the design space, constant parameters, and required model outputs for the generation of the active subspace model. Note that the minimum and maximum values of the fluid parameters are taken from Table 1. Additionally, the range of the degree of reaction is selected in order to guarantee a feasible combination of degree of reaction and specific speed, thus preventing discontinuities in the objective function. The other parameters are selected according to design practices for radial inflow turbines.

3.1. Surrogate of the turbine efficiency function

Errors arising from the numerical solution of the complex system of equations determine a certain scattering of the calculated values of the objective function. Due to this, the determination of the active eigenvectors is performed with an oversampling factor of fifty, which is beyond the customary range (between two and ten). Fig. 6 displays the results of the estimation of **C** associated to the total-to-static efficiency function. As displayed in Fig. 6a, the largest gap among eigenvalues is the first one, suggesting that the reduced-order model might be generated with just a single active variable. However, the second gap is comparatively quite large, indicating the existence of another relevant direction of function variability. The reduced-order function is then made dependent on two active variables; Figs. 6b and c show the corresponding eigenvectors, and Fig. 6d presents the corresponding response surface.

The dotted lines in Figs. 6a-c are bootstrap intervals [17]; they allow to assess the accuracy of the estimation of **C**. These intervals suggest that the computation of the eigenvalues and the first eigenvector are accurate. However, the estimation of the second eigenvector is poor, for the error in the estimate is inversely proportional to the size of the second, smaller, eigenvalue gap. Eventually, this inaccuracy increases the approximation error of the reduced-order model.

Fig. 7a presents the contour plot of the surrogate for the efficiency; Fig. 7b displays the corresponding standard deviation, which includes the dispersion induced by the approximation of the fluid model and the meanline code. These charts are obtained with a minimum of ten samples per each region traced in Fig. 7b. The sampling needed to determine $\hat{\mathbf{C}}$ does not provide enough samples in all the boxes in Fig. 7b; thus, additional sampling must be performed wherever needed. The red areas indicate regions where the surrogate is not valid, because either the meanline code fails, or no active variables exist. The active subspace model features good accuracy, except for few combinations of active

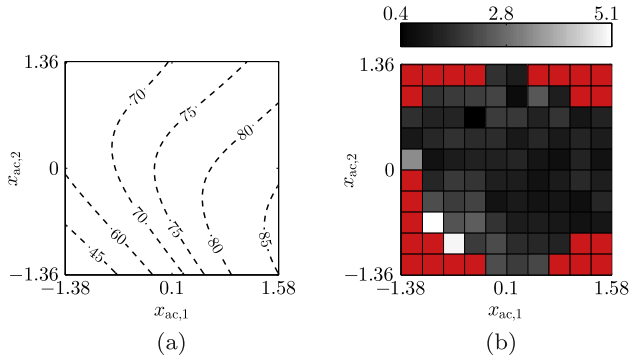

Fig. 7. (a) Contour plot of the reduced-order response surface corresponding to the turbine total-to-static efficiency function. (b) Standard deviation of the surrogate.

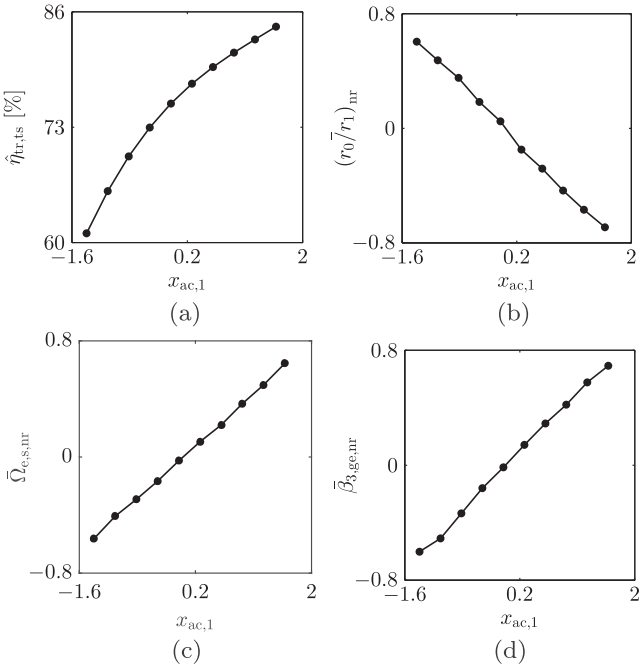

Fig. 8. Total-to-static efficiency, and turbine-related normalized inputs as a function of the first active variable, and taking the second active variable equal to zero: (a) total-to-static efficiency, (b) stator aspect ratio, (c) rotor outlet blade angle, (d) isentropic specific speed. The plots are obtained with 1000 random samples per point.

variables. The same procedure has been successfully applied to all the outputs of interest listed in Table 2. The total time required to generated the surrogate was five hours.

The reduced-order model depicted in Fig. 7a is a polynomial of fourth degree,

$$\begin{aligned}\hat{\eta}_{tr,ts} = &-0.0057225x_{ac,1}^4 - 0.19081x_{ac,1}^3x_{ac,2} + 0.49523x_{ac,1}^3 \\ &- 1.2889x_{ac,1}^2x_{ac,2}^2 + 2.5406x_{ac,1}^2x_{ac,2} - 2.0352x_{ac,1}^2 \\ &- 0.85368x_{ac,1}x_{ac,2}^3 + 3.9847x_{ac,1}x_{ac,2}^2 - 5.1624x_{ac,1}x_{ac,2} \\ &+ 7.214x_{ac,1} + 0.14738x_{ac,2}^4 + 1.7392x_{ac,2}^3 - 5.2157x_{ac,2}^2 \\ &- 1.1701x_{ac,2} + 76.078.\end{aligned} \tag{22}$$

The regression is realized with an automated tool [35]. The large amount of terms allows the function to minimize the deviation in all the active subspace regions.

3.1.1. Relevant design variables: response surface interpretation

The scalar values of the first eigenvector, shown in Fig. 6b, are related to the global sensitivity of the efficiency to the design inputs. The most important turbine design parameters are the ratio of the stator inlet to outlet radii, the specific speed, and the rotor outlet blade angle. The interpretation of the two-dimensional response surface is facilitated by Fig. 8 which displays these variables, and the total-to-static efficiency, as a function of the first active variable, and taking the second active variable equal to zero. The coordinates in Fig. 8 are a result of averaging 1000 random samples per point, hence they represent general trends in the active subspace.

Fig. 8b shows the ratio of stator inlet to outlet radii. A lower value positively affects the turbine efficiency, because it reduces the end-wall area of the stator and the corresponding end-wall losses. The trend of the specific speed features a similar explanation (see Fig. 8c): a higher value increases the stator aspect ratio, thus reducing secondary losses. A further advantage is the reduction of clearance losses. Finally, Fig. 8d shows that a large rotor blade angle is beneficial, because it reduces the leaving swirl and the corresponding rotor exit losses [8].

Fig. 9 presents the corresponding charts for the most influential fluid model parameters: molar mass, acentric factor, and critical temperature. A higher molar mass increases the mass flow rate, the blade height, and the Reynolds number [36]. As a result, higher values improve the turbine efficiency by reducing scaling effects, see Fig. 9a.

Fig. 9b and c display the critical temperature and the acentric factor, respectively; they feature similar trends which are explained by analyzing the stator geometry. For given r_0/r_1 and r_1/r_2, the stator aspect ratio can be calculated as

$$\frac{b_0}{r_0 - r_1} = 2\left(\frac{r_0}{r_1}\frac{r_1}{r_2} - \frac{r_1}{r_2}\right)^{-1}\frac{b_0}{D_2} = K\frac{b_0}{D_2}, \tag{23}$$

where K is a constant. A lower critical temperature and acentric factor increase the saturation pressure and decrease the specific vol-

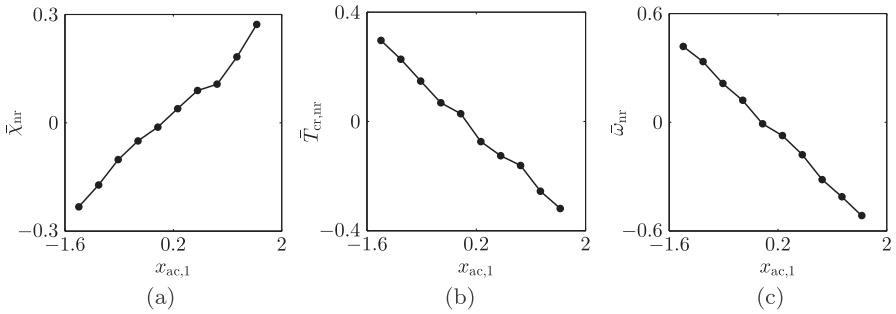

Fig. 9. Fluid-related inputs as a function of the first active variable, and taking the second active variable equal to zero: (a) molar mass, (b) critical temperature, (c) acentric factor. The plots are realized with 1000 random samples per point.

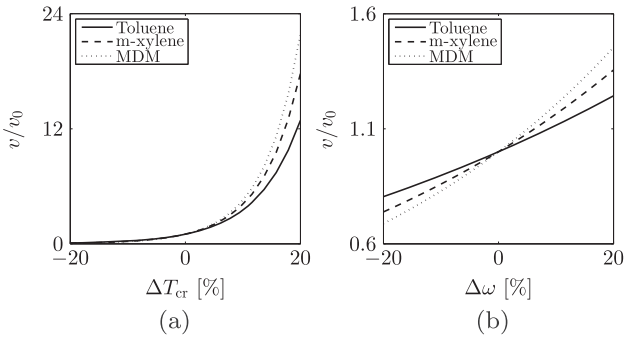

Fig. 10. Change in saturated vapor specific volume as a function of (a) the critical temperature, and (b) the acentric factor, for three exemplary fluids. The specific volume values are computed with a saturation temperature of 80 °C.

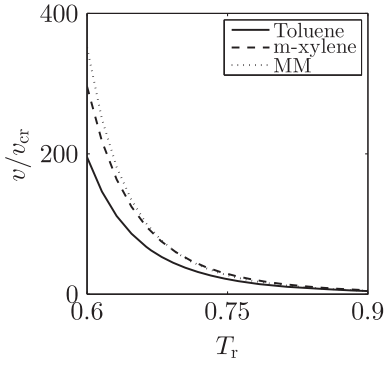

Fig. 11. Ratio of saturated vapor specific volume to critical volume as a function of the reduced temperature, for three exemplary fluids.

ume (e.g., see Fig. 10), thus reducing the blade height and the rotor inlet diameter, which is computed with the volumetric flow at turbine outlet $\dot{m}v_{out,s}$, see (10). However, the diameter decreases more rapidly, because the change of the specific volume $v_{out,s}$ is steeper at lower pressures, see Fig. 11. Consequently, lower values of acentric factor and critical temperature increase the stator aspect ratio and decrease the secondary flows.

It can be concluded that the analysis of the response surface is an effective alternative to the conventional orthogonal sensitivity analysis, for the ranking of the impact of the design parameters on the quantity of interest.

3.2. Application of the surrogate model: a test case

Table 3 shows the constraints employed in the exemplary design optimization of a 10 kW turbine operating in a cycle with an evaporating temperature of 240 °C. These restrictions originate from know-how on the design of radial inflow turbines [33], and from considerations on manufacturing capabilities regarding the minimum blade height.

The optimization procedure explained in Section 2.4 yields several solutions characterized by similar efficiency and power, but employing different working fluids and leading to different turbine

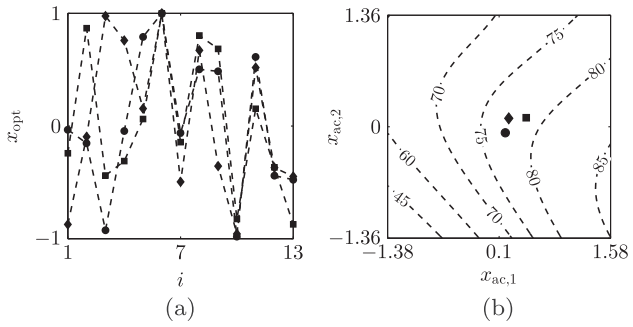

Fig. 12. Solutions of the constrained optimization in (a) the multidimensional space, and in (b) a contour plot of the active subspace. (■) solution corresponding to PP_5.

specifications. It follows that, as already discussed in Ref. [16], all the multidimensional optima belong to a single active subspace region. As an example, Fig. 12 presents the coordinates of three optima in the multidimensional space (Fig. 12a), and in the active subspace (Fig. 12b). Note that the surrogate provides not only the efficiency of the turbine, but also the geometry of the machine and the parameters of the working fluid CEoS.

Fig. 13 shows the main features of the optimal turbines. Since the three solutions feature three different working fluids, the size of the optimal turbines are different, as well as the rotational speed, and their pressure ratio. As a result, the distribution of the loss sources is different, yet the efficiency is the same because the optimal solutions are found in a small active subspace region.

Fig. 14 displays the corresponding thermodynamic cycles in the temperature-entropy diagram of the working fluid associated with the optimal turbine designs. The difference in the cycle thermal efficiency is mostly determined by the values of the critical temperature and molecular complexity of the working fluid [18]. In this case, all design options might be feasible. The selection of a particular design solution depends on aspects related to turbine operation and geometry, and must also take into account other features, e.g., thermal efficiency, evaporating and condensing pressures, dimension and weight of the heat exchangers, etc.

One of the solutions in Figs. 12–14 corresponds to the selection of PP_5 as the working fluid. This substance is selected because its fluid parameters are similar to those corresponding to an optimal solution, thus proving that this method can be used to determine parameters of a non-existing fluid and possibly guide towards the synthesis of new chemicals, or to select existing ones. Alternatively, as demonstrated in the following section, it is possible to perform an optimization by predefining an already existing fluid in the design space.

3.3. Performance of the surrogate model

Fig. 15 displays the results obtained with two different design optimization procedures. In one case, the meanline code is coupled with a genetic algorithm, while the other relies on the use of the active subspace model. In order to perform a fair comparison, the oversampling factor is taken equal to fifty for both methods. Additionally, PP_{90} is selected as the working fluid; the corresponding fluid parameters are then predefined in the design space.

Table 3
Optimization constraints and constant parameters

ϑ, –	φ, –	w_3/w_2, –	b_0, mm	$\dot{W}_{tr}$, kW	T_{ev}, °C
$\leqslant 0.7$	$\geqslant 0.4$	$\geqslant 1.5$	$\geqslant 1.5$	$9.0 \leqslant \dot{W}_{tr} \leqslant 11.0$	240.0

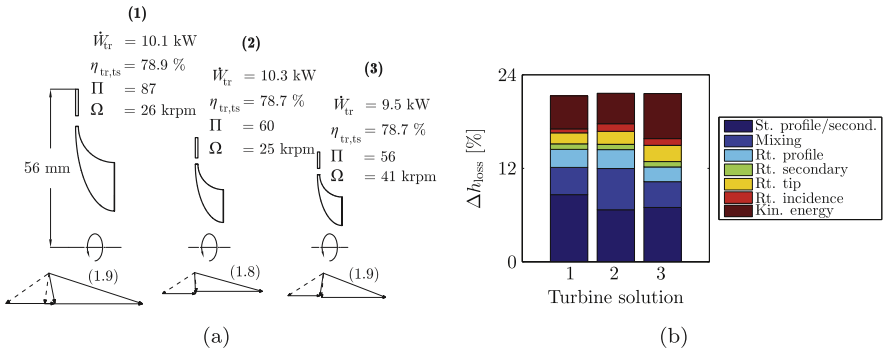

Fig. 13. Solutions of the exemplary constrained design optimization problem: (a) turbine meridional channel and velocity triangles. The number in parenthesis above the velocity triangles correspond to the flow absolute Mach number at rotor inlet. (b) Turbine loss breakdown. Solution (2) is obtained with PP_5 as the working fluid. Design (1) and (3) correspond to turbines operating with non-existing fluids (fluid parameters can be obtained from Table 1.

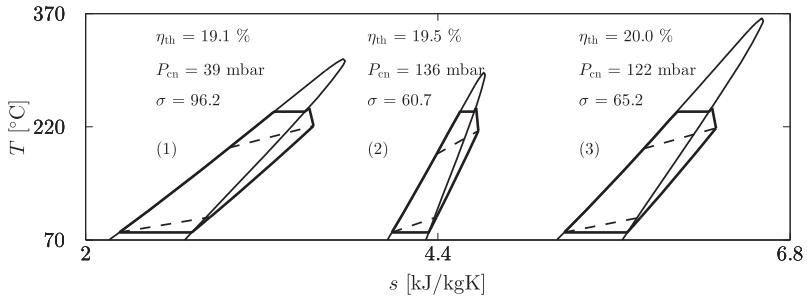

Fig. 14. Solutions of the constrained optimization: temperature-entropy diagram of the thermodynamic cycle. Solution (2) is obtained with PP_5 as the working fluid. The regenerator pinch temperature is 20 K.

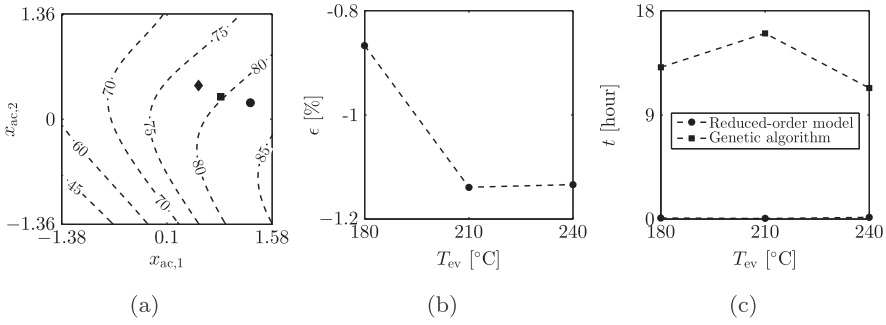

Fig. 15. (a) Optimization results using the active subspace model and PP_{90} as the working fluid: (•) T_{ev} = 180 °C, (■) T_{ev} = 200 °C, (◆) T_{ev} = 240 °C. (b) Deviation between the results given by the surrogate and those given by the genetic algorithm. The deviation is computed like a relative error where the result of the genetic algorithm is the reference. (c) Optimization time, without taking into account the sampling time.

The optimization is performed for three different temperature levels (180 °C, 210 °C, 240 °C), and with the constraints reported in Table 3. Fig. 15a depicts the optima provided by the active subspace model. Fig. 15b illustrates the deviation between the results given by the surrogate and the genetic algorithm. This deviation is computed like a relative error where the result of the genetic algorithm is the reference. The surrogate leads to accurate optimal solutions, regardless the uncertainty introduced by the approximation of the thermodynamic model. Thus, it can be employed to select the optimal working fluid, cycle specifications, and the turbine geometry.

The comparison of the computational time is shown in Fig. 15c. The time referring to the active subspace optimization does not take into account the sampling. The optimization by means of active subspaces is at least two orders of magnitude faster than the conventional procedure based on the meanline code.

4. Concluding remarks

This paper describes a new method to efficiently perform the integrated design of the turbine of power cycles operating with unconventional fluids, and its assessment. The preliminary design procedure integrates the selection of the working fluid, the calculation of the optimal thermodynamic cycle and the sizing of the corresponding optimal turbine. Such a complex mathematical problem has been solved with active subspaces, a mathematical technique yielding a reduced order model that proved to be computationally efficient and robust.

The benefits of the method are demonstrated by its application to the design of a 10 kW *m*ORC unit for the exploitation of medium-temperature thermal sources, and adopting a single-stage radial inflow turbine. The application of the active subspaces to the turbine efficiency function leads to a reduced-order model

constituted by two active variables. Similar results are also obtained for the other outputs of interest (e.g., blade height). Other advantages of the proposed method are:

- The method allows to restrict the search of the global optimum to a small region in terms of active variables. These solutions contain information regarding the turbine geometry, the working fluid parameters, and the thermodynamic cycle operating conditions. If the molecular parameters of the fluid do not correspond to an existing fluid, it can be speculated that further investigation might tell if the molecule can be synthesized.
- The surrogate-based optimization outperforms the standard design approach by providing optimal solutions with a computational cost which is at least two orders of magnitude lower.
- Once the surrogate is available, it can be used to solve any design problem within the boundaries employed to construct the surrogate. The surrogate requires negligible computational effort.
- The response surface can be used to infer which parameters and trends are dominant with respect to turbine performance. In the described example, the most influential design inputs are the stator inlet to outlet radius ratio, the specific speed, and the rotor outlet geometric angle. Likewise, the most important fluid model parameters are the molar mass, the critical temperature, and the acentric factor.

Future developments will include the addition of the preliminary design of the heat exchangers to the procedure. Therefore, it will be possible to evaluate other objective functions, e.g., system cost, weight, volume, etc.

Acknowledgments

The authors are grateful to Bosch GmBH for funding the project that led to the results presented in this article, and for the fruitful discussions with Bernd Banzhaf of the division Diesel Systems, Engineering Component - Simulation and Testing; and Martin Dreizler of the division Corporate Sector Research and Advance Engineering, Future Mechanical and Fluid Components.

References

[1] P. Colonna, E. Casati, C. Trapp, T. Mathijssen, J. Larjola, T. Turunen-Saaresti, A. Uusitalo, Organic Rankine cycle power systems: from the concept to current technology, applications and an outlook to the future, J. Eng. Gas Turb. Power 137 (10) (2015), 100801-1–19.
[2] W. Lang, P. Colonna, R. Almbauer, Assessment of waste heat recovery from a heavy-duty truck engine by means of an ORC turbogenerator, J. Eng. Gas Turb. Power 135 (4) (2013), 042313-1–10.
[3] C. Perullo, D. Mavris, E. Fonseca, An integrated assessment of an organic Rankine cycle concept for use in onboard aircraft power generation, in: ASME Turbo Expo, no. GT2013-95734, 2013, p. 8.
[4] M.E. Mondejar, F. Ahlgren, M. Thern, M. Genrup, Quasi-steady state simulation of an organic Rankine cycle for waste heat recovery in a passenger vessel, Appl. Energy 185 (Part 2) (2017) 1324–1335.
[5] C.D. Servi, L. Azzini, M. Pini, A.G. Rao, P. Colonna, Exploratory assessment of a combined-cycle engine concept for aircraft propulsion, in: Proceedings of the 1st Global Power and Propulsion Forum - GPPF2017, no. GPPF-2017-78, 2017, p. 11.
[6] S. Bahamonde, M. Pini, C. De Servi, P. Colonna, Method for the preliminary fluid dynamic design of high-temperature mini-ORC turbines, J. Eng. Gas Turb. Power 139 (8) (2017) 082606–1–14.
[7] E. Macchi, A. Perdichizzi, Efficiency prediction for axial-flow turbines operating with nonconventional fluids, J. Eng. Power 103 (4) (1981) 718–724.
[8] A. Perdichizzi, G. Lozza, Design criteria and efficiency prediction for radial inflow turbines, in: ASME Gas Turbine Conference and Exhibition, no. 87-GT-231, 1987, p. 9.
[9] A. Toffolo, A. Lazzaretto, G. Manente, M. Paci, A multi-criteria approach for the optimal selection of working fluid and design parameters in organic Rankine cycle systems, Appl. Energy 121 (2014) 219–232.
[10] D. Maraver, J. Royo, V. Lemort, S. Quoilin, Systematic optimization of subcritical and transcritical organic Rankine cycles (ORCs) constrained by technical parameters in multiple applications, Appl. Energy 117 (2014) 11–29.
[11] A. Pezzuolo, A. Benato, A. Stoppato, A. Mirandola, The ORC-PD: a versatile tool for fluid selection and organic Rankine cycle unit design, Energy 102 (2016) 605–620.
[12] E. Casati, S. Vitale, M. Pini, G. Persico, P. Colonna, Centrifugal turbines for mini-organic Rankine cycle power systems, J. Eng. Gas Turb. Power 136 (12) (2014), 122607-1–11.
[13] M. Erbas, A. Biyikoglu, Design and multi-objective optimization of organic Rankine turbine, Int. J. Hydrogen Energy 40 (44) (2015) 15343–15351, The 4th International Conference on Nuclear and Renewable Energy Resources (NURER2014), 26–29 October 2014, Antalya, Turkey.
[14] A. La Seta, A. Meroni, J.G. Andreasen, L. Pierobon, G. Persico, F. Haglind, Combined turbine and cycle optimization for organic Rankine cycle power systems – Part B: Application on a case study, Energies 9 (6) (2016) 393.
[15] R. Aungier, Turbine aerodynamics, axial-flow and radial-inflow turbine design and analysis, ASME, New York, USA, 2006.
[16] S. Bahamonde, M. Pini, P. Colonna, Active subspaces for the preliminary fluid dynamic design of unconventional turbomachinery, in: M. Papadrakakis, V. Papadopoulos, G. Stefanou, V. Plevris (Eds.), European Congress on Computational Methods in Applied Sciences and Engineering, vol. 7806, 2016, p. 15.
[17] P.G. Constantine, Active subspaces: emerging ideas for dimension reduction in parameter studies, SIAM-Soc. Ind. Appl. Math. (2015).
[18] G. Angelino, C. Invernizzi, E. Macchi, Organic Working Fluid Optimization for Space Power Cycles, Springer-Verlag, Berlin, 1991.
[19] G. Angelino, C. Invernizzi, Cyclic methylsiloxanes as working fluids for space power cycles, J. Sol. Energ. - Trans. ASME 115 (3) (1993) 130–137.
[20] E.W. Lemmon, M. Huber, M.O. McLinden, NIST standard reference database 23: Reference fluid thermodynamic and transport properties-REFPROP, version 9.1, national Institute of Standards and Technology, Gaithersburg, 2013. <https://www.nist.gov/srd/refprop>.
[21] P. Colonna, T.P. van der Stelt, A. Guardone, FluidProp (Version 3.0): A program for the estimation of thermophysical properties of fluids, asimptote bv, Delft, The Netherlands, 2012. <http://www.fluidprop.com>.
[22] C.M. Invernizzi, Closed power cycles, in: Lecture Notes in Energy, Vol. 11, Springer-Verlag, London, 2013.
[23] S. Vitale, Preliminary design method for small scale centrifugal orc turbines, Master's thesis, Politecnico di Milano, 2012.
[24] A. Head, C. De Servi, E. Casati, M. Pini, P. Colonna, Preliminary design of the ORCHID: a facility for studying non-ideal compressible fluid dynamics and testing ORC expanders, in: ASME Turbo Expo, no. GT2016-56103, 2016, p. 14.
[25] Various Authors, Matlab version 8.2.0.701 (R2013b), the MathWorks Inc., 2013.
[26] M. Pini, G. Persico, E. Casati, V. Dossena, Preliminary design of a centrifugal turbine for organic Rankine cycle applications, J. Eng. Gas Turb. Power 135 (4) (2013), 042312-1–9.
[27] J.M. Smith, H.C. Van Ness, M.M. Abbot, Introduction to Chemical Engineering Thermodynamics, seventh ed., McGraw-Hill Education, New York, 2005.
[28] J.D. van der Waals, The equation of state for gases and liquids, in: Nobel Lectures, Physics 1901–1921, Elsevier Publishing Company, Amsterdam, 1967, pp. 254–265.
[29] O. Redlich, J.N.S. Kwong, On the thermodynamics of solutions. V. An equation of state. Fugacities of gaseous solutions, Chem. Rev. 44 (1) (1949) 233–244.
[30] D.Y. Peng, D.B. Robinson, A new two-constant equation of state, Ind. Eng. Chem., Fundam. 15 (1) (1976) 59–64.
[31] G. Soave, Equilibrium constants from a modified Redlich-Kwong equation of state, Chem. Eng. Sci. 27 (6) (1972) 1197–1203.
[32] W.C. Reynolds, P. Colonna, Thermodynamics: fundamentals and engineering applications, Cambridge University Press, 2018 (Ch. 7, Vapor Power Plants).
[33] S. Dixon, C. Hall, Fluid Mechanics and Thermodynamics of Turbomachinery, sixth ed., Butterworth-Heinemann, Boston, MA, 2010.
[34] P. Constantine, E. Dow, Q. Wang, Active subspaces mmethod in theory and practice: applications to kriging surfaces, SIAM J. Sci. Comput. 36 (4) (2014) A1500–A1524.
[35] J. D'Errico, Polyfitn - Polynomial Modeling in 1 or n Dimensions, MATLAB Central File Exchange. Retrieved March, 2014, 2012.
[36] H. Tabor, L. Bronicki, Establishing Criteria for Fluids for Small Vapor Turbines, SAE Technical Paper 640823, 1964, pp. 561–575.